

Author Response to Interactive Comment on “Reflection tomography of time-lapse GPR data for studying dynamic unsaturated flow phenomena” by Adam R. Mangel et al.

This response is directed toward the comments left by Anonymous Referee #4, posted to the Hydrology and Earth Systems Science (HESS) discussion board for manuscript hess-2018-230 on August 28, 2019.

The authors would like to thank the reviewer for devoting time to reviewing our manuscript and for expeditiously providing a critical review of the content. Below, the authors have outlined responses to individual comments made by the reviewer.

---

***AR4:** The authors demonstrate the coupling automated GPR data collection with reflection tomography in synthetic studies and laboratory studies. Given a perfect hydrological model for a homogenous soil, the considerable discrepancy (5~10%) between the true water content and the estimates from reflection tomography indicates the proposed approach is not ready for hydrological applications. Further analysis of the accuracy of the tomography approach is needed.*

**Author Response:** This is the first of its kind study which establishes that time-lapse GPR reflection tomography of a dynamic infiltration event is now technically possible, thus establishing a reference point for future studies. The study points out shortcomings of the state-of-the-art in reflection tomography and offers potential solutions which are best explored in detail in later works that can focus on examining these issues. The authors maintain that the findings presented here are important to the hydrogeophysics community as they establish a scientifically sound and robust assessment of the method’s potential and limitations when use in hydrological applications.

***AR4:** Provided such an irrigation setup for surface infiltration, heterogeneous water flow could be expected. I am wondering how these small-scale heterogeneities within a CMP gather influences on the accuracy of the reflection tomography algorithm. Please clarify this.*

**Author Response:** As with any measurement of soil moisture, there are limitations regarding the scale at which heterogeneities can be resolved. For example, the moisture probes used in this work are averaging the volumetric moisture content over a cylindrical volume of roughly 143 cubic centimeters ([Meter Group](#)). Similarly, with GPR methods it is generally accepted that the resolution of the GPR signal is roughly 25% of the wavelength of the signal (see figure 2 of Mangel et al. 2015). The wavelength of the signal for this work is roughly 10 centimeters (varies with velocity/water content). Small-scale heterogeneities are accounted for in this work by using a ray tracing algorithm capable of accounting for these small-scale heterogeneities (curved ray tracer) in the pre-stack depth migration. The dense spacing of the CMPs at 0.2 m also provides repeated measurements of the same volume, increasing the ability of the data to resolve these small changes in soil moisture.

***AR4:** The error (5~10%) in the synthetic studies mainly comes from the artifacts, while the serious error (5~15%) in the laboratory studies might be from improper probe locations. Concerning the foreseeable heterogeneous water flow, the comparison on the reflection tomography estimates with the probes half-meter away might not make sense. Hence, more solid validation is required to consolidate the quantitative characterization of dynamic*

*unsaturated flow phenomena. Finally, the relationships between the two error levels (5~10% vs. 5~15%) should be discussed.*

**Author Response:** We agree with the reviewer that it in an ideal scenario, the moisture probes would be located in the plane of the GPR image and that this offset could be contributing to the observed discrepancies between probes and GPR for the experimental case given the heterogeneous flow that occurred. The moisture probes were located off the GPR transect to avoid backscattering in the transmitted signal that would interfere with analysis of the GPR wave velocities. Though this is not an ideal setup for comparison of the moisture probe data to the GPR estimated of water content, it was necessary to ensure that high-quality reflection tomography data could be collected. We have modified the conclusions to emphasize this point as a potential source of error in the experiment at line 204-205 of the manuscript.

Notably this is not an issue for the numerical experiment, so does not fully explain all of the error in the water content estimates. Therefore, the two main sources of discrepancies between the water content probes and tomography results are likely (i) the lack of a coherent wetting front reflection as seen in numerical experiments reducing the available data for the reflection tomography (i.e., if more reflectors were present, an improved image would like result), and (ii) experimental errors that include discrepancy in effective measurement scale between the inversion and probes, consequences of out of plane probes, or other general experimental errors. We have expanded the discussion on lines 201-209 to elaborate on these issues.

*AR4: The authors just demonstrate the discrepancies between reflection tomography and Probes for three-time slides (0, 95 and 173). Considering the fast evolution of the heterogeneous wetting, I am wondering how the discrepancies evolve.*

**Author Response:** We have addressed a similar comment in earlier reviews of the manuscript.

The authors selected these specific times to illustrate that the reflection tomography does indeed show substantial changes in the water content that are realistic and generally consistent with measurements made at point probes; at least in trend if not in magnitude due to scale issues between the imaging and point sensors.

The work for this manuscript was performed in a seismic imaging software which is engineered to handle large static seismic data sets and involves substantial manual intervention to identify reflections in the data. Processing the data for each time is therefore a substantial burden and we do not have results available from additional times. Furthermore, the software is unable to account for electrical conductivity of the soil and utilizes Kirchoff migration, which the authors identify as a limitation in properly migrating the data.

Despite the fact that of the presented tomography results in time, the selected times greatly enhance the information content of the infiltration process in the spatial domain compared to invasive methods (i.e., probes). The authors plan to continue with this research once a more accessible and hydrogeophysically-oriented software is developed by the lead author, which will substantially increase the efficiency and ability to perform these analyses at a higher temporal discretization, but this is well beyond the scope of this manuscript.

**Mineral comments:**

**AR4:** L40-41: *I didn't find a multi-offset survey for infiltration experiment in Gerhards (2008). Besides, the journal name is missing in the reference.*

**Author Response:** Figure 1 of the Gerhards et al (2008) paper shows GPR acquisition setup. From the figure, it can be seen that data are being collected at multiple antenna offsets, which they refer to as multi-channel.

The journal for the reference is Geophysics, which is properly cited in the bibliography on line 245 of the PDF version of the second revision of the submitted manuscript (uploaded Feb 28, 2019).

**AR4:** L124: *'mS/m' to 'mS m-1'.*

**Author Response:** The change has been incorporated into the new revision of the manuscript.

**AR4:** L134: *'Reflection TOMography Of simulations' to 'Reflection Tomography of Simulations'*

**Author Response:** The heading for section 3 of the manuscript is correct in the PDF version of the second revision of the submitted manuscript (uploaded Feb 28, 2019).

**AR4:** Line 219: *The format of paper title should be just capitalized the first word. Same issue for other references.*

**Author Response:** The change has been incorporated in the new revision of the manuscript.

Author Response to Interactive Comment on “Reflection tomography of time-lapse GPR data for studying dynamic unsaturated flow phenomena” by Adam R. Mangel et al.

This response is directed toward the comments left by Referee #5, Timothy Bechtel, posted to the Hydrology and Earth Systems Science (HESS) discussion board for manuscript hess-2018-230 on October 16, 2019.

The authors would like to thank the reviewer for devoting time to reviewing our manuscript and for expeditiously providing a critical review of the content. The authors also recognize the reviewer for identifying themselves as they view this as a step forward in a truly open manuscript review process. Below, the authors have outlined responses to individual comments made by the reviewer.

---

We have accepted all typographic suggestions made by the reviewer and incorporated them into the revision of the manuscript.

# 1 Reflection tomography of time-lapse GPR data for studying 2 dynamic unsaturated flow phenomena

3 Adam R. Mangel<sup>1,2</sup>, Stephen M.J. Moysey<sup>2</sup>, John Bradford<sup>1</sup>

4 <sup>1</sup> Department of Geophysics, Colorado School of Mines, Golden, Colorado, 80401, USA

5 <sup>2</sup> Department of Environmental Engineering and Earth Science, Clemson University, Clemson, South Carolina, 29634,  
6 USA

7 Corresponding to: Adam R. Mangel (amangel@mines.edu)

## 9 Abstract

10 Ground-penetrating radar (GPR) reflection tomography algorithms allow non-invasive monitoring of water content  
11 changes resulting from flow in the vadose zone. The approach requires multi-offset GPR data that **are** traditionally  
12 slow to collect. We automate GPR data collection to reduce the survey time significantly, thereby making this  
13 approach to hydrologic monitoring feasible. The method was evaluated using numerical simulations and laboratory  
14 experiments that suggest reflection tomography can provide water content estimates to within 5%-10% vol. ~~vol.~~<sup>1</sup> for  
15 the synthetic studies, whereas the empirical estimates were typically within 5%-15% of measurements from in-situ  
16 probes. Both studies show larger observed errors in water content near the periphery of the wetting front, beyond  
17 which additional reflectors were not present to provide data coverage. Overall, coupling automated GPR data  
18 collection with reflection tomography provides a new method for informing models of subsurface hydrologic  
19 processes and a new method for determining transient 2D soil moisture distributions.

Formatted: Superscript

## 20 1. Introduction

21 Preferential flow is ubiquitous in the vadose zone, occurring under a wide variety of conditions and over a  
22 broad range of scales (Nimmo, 2012). Reviews such as those by Hendrickx and Flury (2001) and Jarvis (2007)  
23 illustrate that a basic mechanistic understanding of preferential flow exists. Jarvis et al. (2016) point out, however,  
24 that we still lack models capable of reproducing empirical observations in the field and highlight the importance of  
25 non-invasive imaging techniques for improving this understanding. We suggest that ground-penetrating radar (GPR)  
26 reflection tomography could fill this need by quantitatively mapping changes in water content through space and time  
27 at the sub-meter scale.

28 Reflection GPR is commonly used to image subsurface structures, but is also well suited to understanding  
29 hydrologic variability due to the strong dependence of EM wave velocities on soil volumetric water content (Topp et  
30 al., 1980). As a result, GPR has been adapted to monitor variability in hydrologic processes at multiple scales through  
31 time and space in a variety of contexts (Buchner et al., 2011; Busch et al., 2013; Guo et al., 2014; Haarder et al., 2011;  
32 Lunt et al., 2005; Mangel et al., 2012, 2015b, 2017; Moysey, 2010; Saintenoy et al., 2007; Steelman and Endres, 2010;  
33 Vellidis et al., 1990). Note that GPR methods are not applicable in media with relatively high electrical conductivity.

34 While these studies have illustrated a variety of techniques for monitoring changes in water content within  
35 the subsurface, they have generally required assumptions to constrain the interpretation, such as the use of *a priori*  
36 information regarding subsurface structure (e.g., Lunt et al., 2005) or the GPR wave velocity (Haarder et al., 2011).

37 These limitations arise from the fact that GPR data are recorded as energy arriving at the receiver antenna as a function  
38 of time. Inherent assumptions therefore exist in analyzing traveltime data collected with antennas separated by a fixed  
39 offset because both the distance travelled by the GPR wave to a reflector and the velocity of the GPR wave are  
40 unknown. It has been demonstrated that GPR data collected via a multi-offset survey can constrain both the depth to  
41 a moving wetting front and the water content behind the front over the course of an infiltration event (Gerhards et al.,  
42 2008; Mangel et al., 2012). The limitation of these studies, however, was that the authors assumed a 1D flow system  
43 and that GPR data lacked information regarding lateral variability in soil moisture.

44 Extending multi-offset techniques (Forte and Pipan, 2017; Jaumann and Roth, 2017; Klenk et al., 2015;  
45 Lambot et al., 2004, 2009) to image flow in the vadose zone requires an increase in the speed at which these data can  
46 be collected and advanced processing methods that can combine thousands of measurements into spatially and  
47 temporally variable water content estimates. We have recently overcome the data collection problem by automating  
48 GPR data collection using a computer controlled gantry, thereby reducing the data collection time for large multi-  
49 offset surveys from hours to minutes (Mangel et al., 2015a). Tomography and wave migration algorithms from  
50 seismic literature have been available for decades (Baysal et al., 1983; Lafond and Levander, 1993; Sava and Biondi,  
51 2004a, 2004b; Stork, 1992; Yilmaz and Chambers, 1984) and are being continually adapted to GPR applications. For  
52 example, this work is made possible due to adaptation of the pre-stack migration algorithm (Leparoux et al., 2001)  
53 and adaptation of the reflection tomography algorithm (Bradford, 2006) to multi-offset GPR data. Subsequent studies  
54 have demonstrated the use of GPR reflection tomography for imaging static distributions of subsurface water content  
55 with great detail (Bradford, 2008; Bradford et al., 2009; Brosten et al., 2009). The combination of automated GPR  
56 data collection and reflection tomography makes time-lapse imaging of water content during infiltration a feasible  
57 means to study flow in the vadose zone.

58 The objective of this study is to evaluate reflection tomography of high-resolution GPR data as a tool for  
59 observing and characterizing unsaturated flow patterns during infiltration into a homogeneous soil. To evaluate the  
60 efficacy of the algorithm for resolving dynamic soil water content in 2D, we first test the algorithm using numerical  
61 simulations and compare the results to true water content distributions. We then apply the algorithm to time-lapse  
62 GPR data collected during an infiltration and recovery event in a homogeneous soil and compare results to  
63 measurements from in-situ soil moisture probes.

## 64 **2. Methods**

### 65 **2.1. The Reflection Tomography Algorithm**

66 The goal of reflection tomography is to determine a velocity model that best aligns migrated reflection  
67 arrivals for a common reflection point across a set of source-receiver offsets. For brevity, we will limit our discussion  
68 here to the key ideas and methods of the tomography algorithm; we refer the reader to Stork (1992) for the original  
69 tomography algorithm and to Bradford (2006) for the application to GPR data.

70 The data required for this algorithm are an ensemble of common-midpoint (CMP) gathers collected along a  
71 path. Given that GPR data is a time-series record of electromagnetic energy arriving at a point in space, we must  
72 know the proper velocity structure to migrate the data and produce a depth registered image of the GPR energy.  
73 Migration attempts to remove the hyperbolic trend of reflections with respect to antenna offset (Figure 1a) by using

74 the wave velocity to reposition reflections to the proper depth at which they occur. If CMP data are migrated with the  
75 correct velocity, reflections from layers in the subsurface are flattened as a function of offset (Fig. 1c). If the velocity  
76 estimate is incorrect, e.g. 10% too slow (Fig. 1b) or 10% too fast (Fig. 1d), the arrival is not flat and exhibits residual  
77 moveout (RMO). To solve for the velocity structure and properly migrate the data, the reflection tomography  
78 algorithm proceeds as follows (Bradford, 2006; Stork, 1992):

- 79 1. Generate a starting depth vs. velocity model.
- 80 2. Migrate the data with the starting velocity model and stack the data.
- 81 3. Pick horizons on the stacked image.
- 82 4. Perform ray-tracing to the picked horizons with the velocity model.
- 83 5. Evaluate horizons for residual moveout.
- 84 6. Adjust velocity model using reflection tomography.
- 85 7. Apply revised velocity model using migration and quality check RMO.
- 86 8. Iterate at step three if necessary.

87 For this work, starting velocity models for the tomography algorithm are determined by smoothing results  
88 from 1D velocity analysis of individual CMPs (Neidell and Taner, 1971). The reflection tomography algorithm then  
89 adjusts the velocity distribution until reflections in the depth corrected (i.e., migrated) data line up to produce a  
90 reflection at a consistent depth across all traces in a CMP. Through sequential iterations of the tomographic inversion,  
91 the RMO metric is reduced on a global scale. For this work, the reflection tomography was performed using the  
92 SeisWorks software suite and Kirchhoff pre-stack depth migration (Yilmaz and Doherty, 2001).

## 93 2.2. Experimental Setup and Procedure

94 We used a 4 m x 4 m x 2 m tank for the controlled study of unsaturated flow phenomenon with GPR (Fig.  
95 1e, f). We filled the tank with a medium-grained sand to a depth of 0.60 m. Below the sand was a 0.30 m layer of  
96 gravel that acts as backfill for 16 individual drain cells that are pitched slightly toward central drains that route water  
97 to outlets on the outside of the tank. We constructed an automated data collection system to allow for the high-speed  
98 high-resolution collection of GPR data (Mangel et al., 2015a); the GPR gantry fits inside of the tank so the antennas  
99 are in contact with the sand surface. All GPR data described here were collected along the y-axis of the tank at a fixed  
100 position of  $x = 2.0$  m, where the bottom of the tank is flat (Fig. 1e, f).

101 The automated system, which utilizes a 1000 MHz ~~Sensors and Software~~ bistatic radar (Sensors and  
102 Software, Inc.), was operated to obtain 101 CMPs spaced at 0.02 m intervals between  $y = 1.0$  m - 3.0 m. Each CMP  
103 consisted of 84 traces with offsets between 0.16 m-1.0 m at 0.01 m step size. Thus, a complete CMP data set for one  
104 observation time consists of almost 8,500 individual GPR traces. With this configuration using the automated system,  
105 a CMP at a single location could be collected in 1.8 seconds with a total cycle of CMP data locations collected every  
106 3.9 minutes.

107 GPR data collection occurred prior to irrigation to evaluate background conditions. Data collection continued  
108 during irrigation, which was applied at a flux of  $0.125 \text{ cm}^3/\text{min}^2$  for a duration of 2.13 hrs. Spatial heterogeneity in  
109 the applied flux has been observed in laboratory testing of the irrigation equipment. Fifteen EC-5 soil moisture probes  
110 (METER, Inc.) logged volumetric water content at 10-second intervals during the experiment (Fig. 1e, f). Note that

Formatted: Superscript

111 the soil moisture probes are located out of the plane of the GPR line by 0.5 m (Figure 1f). GPR data collection  
112 continued for 40 minutes after the irrigation was terminated. In total, 45 complete sets of data were collected over  
113 the course of the 3-hour experiment, yielding more than 500,000 GPR traces in the experimental data set.

### 114 2.3. Execution of the Numerical Simulations

115 We employed HYDRUS-2D (Simunek and van Genuchten, 2005) to simulate a theoretical and realistic  
116 hydrologic response to an infiltration event using two different initial conditions: i) hydrostatic equilibrium leading to  
117 a water content distribution controlled by the soil water retention curve, and ii) a uniform soil with a water content of  
118 0.07. We selected the Mualem-van Genuchten soil model (Mualem, 1976) and parameterized the model as follows  
119 based on hydraulic testing of the sand: residual water content ( $\theta_r$ ) = 0.06, saturated water content ( $\theta_s$ ) = 0.38, air-entry  
120 pressure ( $\alpha$ ) = 0.058 cm<sup>-1</sup>, shape parameter ( $n$ ) = 4.09, and saturated hydraulic conductivity ( $K_s$ ) = 4.6 cm min<sup>-1</sup>. The  
121 hydraulic conductivity for the homogeneous model was reduced to 1 cm min<sup>-1</sup> to build a larger contrast of water  
122 content across the wetting front. For all HYDRUS simulations, we used a constant flux boundary condition of 0.125  
123 cm<sup>3</sup>min<sup>-1</sup> from  $y = 1.6$  m - 2.4 m along the ground surface, set the model domain depth to 0.6 m, length to 4.0 m, and  
124 nominal cell size to 0.04 m. Remaining nodes at the surface were set to no flow boundaries and lower boundary nodes  
125 were set to a seepage face with the pressure head equal to zero.

Formatted: Superscript

126 We calculated relative dielectric permittivity values for the GPR simulations by transforming water content values  
127 from HYDRUS-2D using the Topp equation (Topp et al., 1980). We used the magnetic permeability of free space for  
128 the entire model domain and set electrical conductivity of the soil to 1 mS/m. Although electrical conductivity  
129 changes as a function of the water content, these changes primarily influence wave attenuation, which is not significant  
130 or accounted for in the processing performed with the SeisWorks software.

Formatted: Superscript

131 We performed GPR simulations in MATLAB using a 2D finite-difference time-domain code (Irving and  
132 Knight, 2006). The GPR model domain was set to 4.0 m long and 1.1 m high with a cell size of 0.002 m. The lower  
133 0.3 m of the domain was set to a relative dielectric permittivity of 2.25 to represent the lower gravel layer and the  
134 upper 0.2 m was modeled as air to simulate the air-soil interface. Simulated data were collected as described in the  
135 section detailing the tank experiment. For quick computation, simulations were deployed on the Palmetto  
136 supercomputer cluster at Clemson University, where single source simulations ran in 20 minutes using nodes with 8  
137 CPUs and 32 GB of RAM.

### 138 3. Reflection Tomography of Simulations

139 The HYDRUS-2D output shows the development of an infiltrating wetting front for the two scenarios with  
140 differing initial conditions (Figs. 2a, f, k). For conditions prior to irrigation, the bottom of sand reflection (B) is  
141 horizontal on the common-offset profile (COP) data indicating a constant velocity across the model domain (Fig. 2b).  
142 Additionally, the CMPs show identical hyperbolic moveout, i.e., the offset vs. travelttime relationship, indicating a  
143 homogeneous velocity across the model domain (Fig. 2c-e). The airwave and groundwave are also visible in the data,  
144 but are not analyzed, or further discussed.

145 During infiltration, (B) is distorted at the center of the COP due to the decreased velocity caused by the  
146 infiltrating water (Figs. 2g, l). A reflection from the infiltrating wetting front (W) is faintly visible for the model with  
147 variable initial water contents (Fig. 2g) and comparatively strong for simulations with a dry background (Fig. 2l) due



148 to different levels of dielectric contrast across the wetting front in each case. CMPs also indicate perturbations in the  
149 velocity field as the moveout changes dramatically when the wetted zone is encountered (Figs. 2h-j, m-o). A refraction  
150 is also observed on the CMPs, which is a rare occurrence considering that GPR wave velocity typically decreases with  
151 depth.

152 Prior to the onset of flow, the reflection tomography algorithm produces a uniform water content distribution  
153 that agrees with the arithmetic average of the true water content but does not capture the vertical gradation observed  
154 in Figure 3a. This is because information regarding vertical velocity variations is absent, i.e., more reflectors at  
155 different depths are required to capture this variability. As a result, errors in the water content estimation exceed 10%  
156 vol. % (Fig. 3d).

157 During infiltration, the wetting front is imaged relatively well for the case where the soil was initially dry  
158 (Figs. 3i-l), particularly as the plume advances deeper into the subsurface (Figs. 3m-p) where there is improved data  
159 coverage. The tomography algorithm overestimates the depth of the wetting front by roughly 0.10 m for the case  
160 presented in Figure 3i-l, which is likely due to smoothing effects required to regularize the inversion or an error in the  
161 picking of the wetting front horizon. Considerable errors in the tomography results persist, however, with the results  
162 degrading further for the scenario with variable initial water content (Figs. 3e-h) given that reflection contrasts with  
163 the wetting front are weaker. The presence of an additional reflector, however, increases the ability of the tomography  
164 to resolve vertical variability, e.g. Figure 2g vs. Figure 2b. Overall, errors are reduced near reflectors to about 5% vol.  
165 % (Fig. 3). These results suggest that water content changes resulting from unsaturated flow can be imaged and that as  
166 more information becomes available in the form of additional reflections, the tomography results improve.

Formatted: Superscript

Formatted: Superscript

#### 167 4. Reflection Tomography of Experimental Data

168 At initial conditions, the sand layer reflection (B) is visible at 10 ns traveltimes in the COP collected over the  
169 imaging area (Fig. 4a). Normal hyperbolic moveout of (B) is observed on the CMPs (Fig. 4b, c, d). These results are  
170 qualitatively identical to observations from numerical simulations (Figs. 2b-e).

171 During infiltration, the water content of the sand layer increases substantially (Fig. 5) and longer traveltimes  
172 are observed near the center of the tank (Figs. 4f, i). Rather than a coherent reflection  
173 for the wetting front (W) (Fig. 2l), multiple discrete reflections are present in the COP data (Fig. 4e, i, m) indicating  
174 a heterogeneous wetting of the soil. These reflections are difficult to identify on the CMPs given the complex moveout  
175 pattern (Fig. 4i) but are more easily identified in animations of COP projections of the data (included as a  
176 supplementary file). Analysis of the data was greatly aided by the animation of the data and the pre-stack migration  
177 algorithm, which stacks the data over all offsets to produce a coherent image of reflectors with an increased signal to  
178 noise ratio. Heterogeneous wetting of the soil is also very pronounced in the soil-moisture probe data with many of  
179 the probes responding out of sequence with depth (Fig 5). After irrigation, the soil moisture probes show a decrease  
180 in the soil water content (Fig. 5) apart from one probe (Fig. 5c) and the GPR data show a slight decrease in the  
181 traveltimes of the bottom of sand reflection (Figs. 4k-n).

182 The tomographic imaging results from the initial GPR data set collected prior to irrigation agree with data  
183 from soil moisture probes which indicates an average soil moisture of roughly 5% during this time (Figs. 4e, 5).  
184 During infiltration and recovery, tomographic images of the tank show a wet zone at the center and relatively dry

185 edges outside the irrigated area (Figs. 4j, o). Overall, the tomography results near the center of the tank are within  
186 10% ~~vol./vol.vol. vol.<sup>-1</sup>~~ of the soil moisture data and show a non-uniform wetting of the soil during infiltration that  
187 was not observed in the numerical study, suggesting the occurrence of preferential flow. Errors in the estimates of  
188 water content near the edges of the advancing plume exceed 15% ~~vol./vol.vol. vol.<sup>-1</sup>~~ (Fig. 4b, c), though the general  
189 patterns in wetting are consistent. After irrigation, the tomography results on the edges of the wetted zone are in better  
190 agreement with the soil moisture probe data, but less spatial information is available given the lack of a wetting front  
191 reflection (Fig. 4o).

Formatted: Superscript

Formatted: Superscript

## 192 5. Conclusions

193 Reflection tomography in the post-migrated domain is a viable method for resolving transient soil moisture  
194 content in 2D associated with an infiltration and recovery event in a homogeneous soil. Reflection tomography of  
195 numerical data produced water content distributions that were in good agreement with true water content values from  
196 the simulations. The tomography was generally able to match the true water content values to within 5% -10% vol.  
197 ~~vol.<sup>-1</sup>~~. However, distinct migration artifacts were produced around the edges of the wetting front, especially for cases  
198 where the initial water content was non-uniform, obscuring details about the shape of the wetted region. Analysis of  
199 data collected in a sand tank proved to be more difficult, however, the tomography was able to produce hydrologically  
200 realistic distributions of water content in space and time that were generally within 5% -15% ~~vol./vol.vol. vol.<sup>-1</sup>~~ of  
201 measurements from in-situ soil moisture probes. These discrepancies is may have to do with reduction in available  
202 reflections for analysis caused by the heterogeneous flow response compared to the coherent wetting front reflection  
203 seen in the numerical experiment, e.g. the complex distribution of the wetted soil as a result of heterogeneous  
204 distribution of water at the surface, texture variability in the soil, or other preferential flow mechanisms (Jarvis et al.,  
205 2016). The distance between the location of the CMPs and the moisture probes and the difference in measurement  
206 scale between the two methods may also be a source of these discrepancies given the evidence of non-uniform flow.  
207 Regardless, the fact that the GPR data were able to capture this heterogeneity is an impressive feat given that  
208 tomographic imaging operated independently of any hydrologic information and provided evidence that our  
209 conceptual model was not representative of the physical system.

Formatted: Superscript

Formatted: Superscript

210 Regardless of discrepancies observed between the GPR and probe water content values, it is evident that  
211 automated high-speed GPR data acquisition coupled with reflection tomography algorithms can provide a new  
212 approach to hydrologic monitoring. Testing and revision of conceptual hydrologic models regarding non-uniform  
213 flow in the vadose zone demands such non-invasive time-lapse imaging data. Artifacts observed in the numerical  
214 simulation results, however, suggest that improvements in this methodology could be achieved. While there are likely  
215 fundamental limitations to the information content of the data, the Kirchhoff pre-stack depth migration algorithm used  
216 in this study could be replaced by more sophisticated algorithms like reverse-time migration (Baysal et al., 1983)  
217 which may reduce the observed imaging artifacts. Additionally, results from the tomography algorithm may prove to  
218 be beneficial as a precursor to higher-order inversion techniques, like full-waveform inversion, which requires detailed  
219 starting models of velocity for convergence. Overall, coupling automated GPR data collection with reflection  
220 tomography provides a new method for informing models of subsurface hydrologic processes and a new method for  
221 determining transient 2D soil moisture distributions.

222 **6. Acknowledgements**

223 This material is based upon work supported by, or in part by, the National Science Foundation under grant  
224 number EAR-1151294. We also acknowledge Clemson University for generous allotment of compute time on  
225 Palmetto cluster. Data used in this publication and a supplementary movie of the data are available through the  
226 Colorado School of Mines at the following URL: <https://hdl.handle.net/11124/172053>.

227 **7. References**

- 228 Baysal, E., Kosloff, D. and Sherwood, J.: Reverse Time Migration, *Geophysics*, 48(11), 1514–1524,  
229 doi:10.1190/1.1441434, 1983.
- 230 Bradford, J. H.: Applying reflection tomography in the postmigrated domain to multifold ground-penetrating radar  
231 data, *Geophysics*, 71(1), K1–K8, doi:10.1190/1.2159051, 2006.
- 232 Bradford, J. H.: Measuring **w**Water **c**Content **h**Heterogeneity **u**Using **m**Multifold GPR with **r**Reflection **t**Tomography,  
233 *Vadose Zo. J.*, 7(1), 184, doi:10.2136/vzj2006.0160, 2008.
- 234 Bradford, J. H., Clement, W. P. and Barrash, W.: Estimating porosity with ground-penetrating radar reflection  
235 tomography: A controlled 3-D experiment at the Boise Hydrogeophysical Research Site, *Water Resour. Res.*, 45(4),  
236 n/a-n/a, doi:10.1029/2008WR006960, 2009.
- 237 Brosten, T. R., Bradford, J. H., McNamara, J. P., Gooseff, M. N., Zarnetske, J. P., Bowden, W. B. and Johnston, M.  
238 E.: Multi-offset GPR methods for hyporheic zone investigations, *Near Surf. Geophys.*, 7, 244–257, 2009.
- 239 Buchner, J. S., Kuhne, A., Antz, B., Roth, K. and Wollschlager, U.: Observation of volumetric water content and  
240 reflector depth with multichannel ground-penetrating radar in an artificial sand volume, 2011 6th Int. Work. Adv. Gr.  
241 Penetrating Radar, 1–5, doi:10.1109/IWAGPR.2011.5963910, 2011.
- 242 Busch, S., Weihermüller, L., Huisman, J. A., Steelman, C. M., Endres, A. L., Vereecken, H. and van der Kruk, J.:  
243 Coupled hydrogeophysical inversion of time-lapse surface GPR data to estimate hydraulic properties of a layered  
244 subsurface, *Water Resour. Res.*, 49(12), 8480–8494, doi:10.1002/2013WR013992, 2013.
- 245 Forte, E. and Pipan, M.: Review of multi-offset GPR applications: Data acquisition, processing and analysis, *Signal*  
246 *Processing*, 132, 1–11, doi:10.1016/j.sigpro.2016.04.011, 2017.
- 247 Gerhards, H., Wollschläger, U., Yu, Q., Schiwek, P., Pan, X. and Roth, K.: Continuous and simultaneous  
248 measurement of reflector depth and average soil-water content with multichannel ground-penetrating radar,  
249 *Geophysics*, 73(4), 15–23, 2008.
- 250 Gloaguen, E., Chouteau, M., Marcotte, D. and Chapuis, R.: Estimation of hydraulic conductivity of an unconfined  
251 aquifer using cokriging of GPR and hydrostratigraphic data, *J. Appl. Geophys.*, 47(2), 135–152, doi:10.1016/S0926-  
252 9851(01)00057-X, 2001.
- 253 Guo, L., Chen, J. and Lin, H.: Subsurface lateral preferential flow network revealed by time-lapse ground-penetrating  
254 radar in a hillslope, *Water Resour. Res.*, 50, 9127–9147, doi:10.1002/2013WR014603, 2014.
- 255 Haarder, E. B., Looms, M. C., Jensen, K. H. and Nielsen, L.: Visualizing Unsaturated Flow Phenomena Using High-  
256 Resolution Reflection Ground Penetrating Radar, *Vadose Zo. J.*, 10(1), 84, doi:10.2136/vzj2009.0188, 2011.
- 257 Hendrickx, J. M. H. and Flury, M.: Uniform and Preferential Flow Mechanisms in the Vadose Zone, in *Conceptual*  
258 *Models of Flow and Transport in the Fractured Vadose Zone*, pp. 149–187, National Academy Press, Washington,

259 D.C., 2001.

260 Irving, J. and Knight, R.: Numerical modeling of ground-penetrating radar in 2-D using MATLAB, *Comput. Geosci.*,  
261 32(9), 1247–1258, doi:10.1016/j.cageo.2005.11.006, 2006.

262 Jarvis, N., Koestel, J. and Larsbo, M.: Understanding Preferential Flow in the Vadose Zone: Recent Advances and  
263 Future Prospects, *Vadose Zo. J.*, 15(12), 0, doi:10.2136/vzj2016.09.0075, 2016.

264 Jarvis, N. J.: A review of non-equilibrium water flow and solute transport in soil macropores: Principles, controlling  
265 factors and consequences for water quality, *Eur. J. Soil Sci.*, 58(3), 523–546, doi:10.1111/j.1365-2389.2007.00915.x,  
266 2007.

267 Jaumann, S. and Roth, K.: Soil hydraulic material properties and subsurface architecture from time-lapse GPR,  
268 *Hydrol. Earth Syst. Sci. Discuss.*, (September), 1–34, doi:10.5194/hess-2017-538, 2017.

269 Klenk, P., Jaumann, S. and Roth, K.: Quantitative high-resolution observations of soil water dynamics in a complicated  
270 architecture using time-lapse ground-penetrating radar, *Hydrol. Earth Syst. Sci.*, 19(3), 1125–1139, doi:10.5194/hess-  
271 19-1125-2015, 2015.

272 Lafond, C. F. and Levander, A. R.: Migration moveout analysis and depth focusing, *Geophysics*, 58(1), 91–100,  
273 doi:10.1190/1.1443354, 1993.

274 Lambot, S., Antoine, M., van den Bosch, I., Slob, E. C. and Vanclooster, M.: Electromagnetic Inversion of GPR  
275 Signals and Subsequent Hydrodynamic Inversion to Estimate Effective Vadose Zone Hydraulic Properties, *Vadose  
276 Zo. J.*, 3(4), 1072, doi:10.2136/vzj2004.1072, 2004.

277 Lambot, S., Slob, E., Rhebergen, J., Lopera, O., Jadoon, K. Z. and Vereecken, H.: Remote Estimation of the Hydraulic  
278 Properties of a Sand Using Full-Waveform Integrated Hydrogeophysical Inversion of Time-Lapse, Off-Ground GPR  
279 Data, *Vadose Zo. J.*, 8(3), 743, doi:10.2136/vzj2008.0058, 2009.

280 Leparoux, D., Gibert, D. and Cote, P.: Adaptation of prestack migration to multi-offset ground-penetrating radar  
281 (GPR) data, *Geophys. Prospect.*, 49(3), 374–386, doi:10.1046/j.1365-2478.2001.00258.x, 2001.

282 Lunt, I. A., Hubbard, S. S. and Rubin, Y.: Soil moisture content estimation using ground-penetrating radar reflection  
283 data, *J. Hydrol.*, 307(1–4), 254–269, doi:10.1016/j.jhydrol.2004.10.014, 2005.

284 Mangel, A. R., Moysey, S. M. J., Ryan, J. C. and Tarbuton, J. A.: Multi-offset ground-penetrating radar imaging of  
285 a lab-scale infiltration test, *Hydrol. Earth Syst. Sci.*, 16(11), doi:10.5194/hess-16-4009-2012, 2012.

286 Mangel, A. R., Lytle, B. A. and Moysey, S. M. J.: Automated high-resolution GPR data collection for monitoring  
287 dynamic hydrologic processes in two and three dimensions, *Lead. Edge*, 34(2), doi:10.1190/le34020190.1, 2015a.

288 Mangel, A. R., Moysey, S. M. J. and van der Kruk, J.: Resolving precipitation induced water content profiles by  
289 inversion of dispersive GPR data: A numerical study, *J. Hydrol.*, 525, 496–505, doi:10.1016/j.jhydrol.2015.04.011,  
290 2015b.

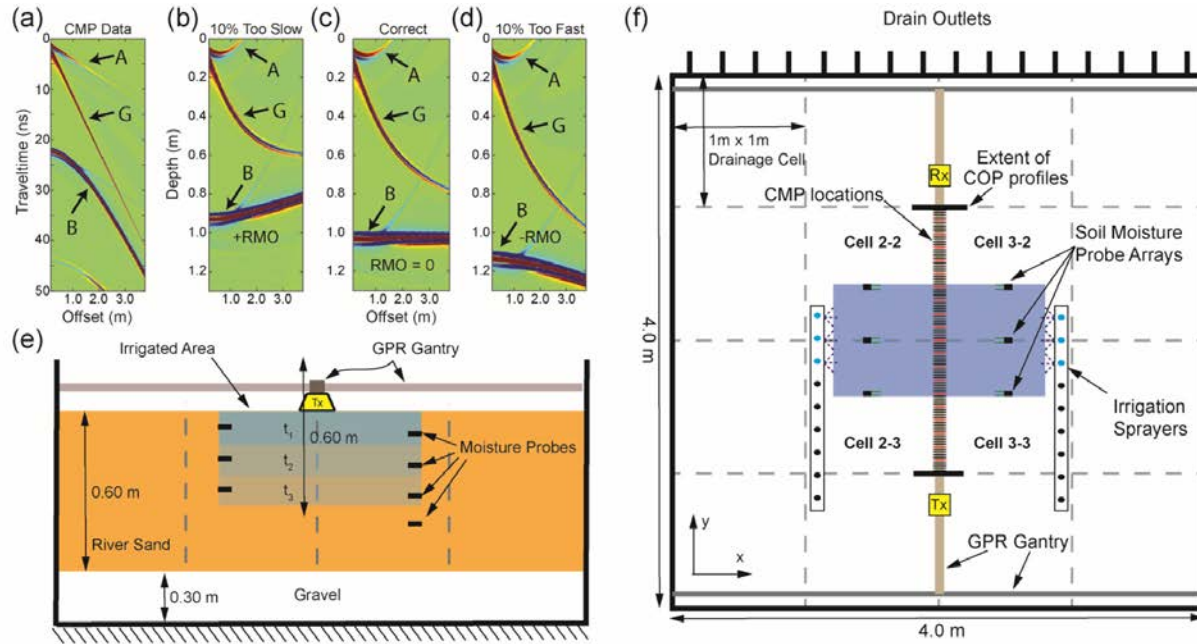
291 Mangel, A. R., Moysey, S. M. J. and van der Kruk, J.: Resolving infiltration-induced water content profiles by  
292 inversion of dispersive ground-penetrating radar data, *Vadose Zo. J.*, 16, doi:10.2136/vzj2017.02.0037, 2017.

293 Moysey, S. M.: Hydrologic trajectories in transient ground-penetrating-radar reflection data, *Geophysics*, 75(4),  
294 WA211-WA219, doi:10.1190/1.3463416, 2010.

295 Mualem, Y.: A new model for predicting the hydraulic conductivity of unsaturated porous media, *Water Resour. Res.*,

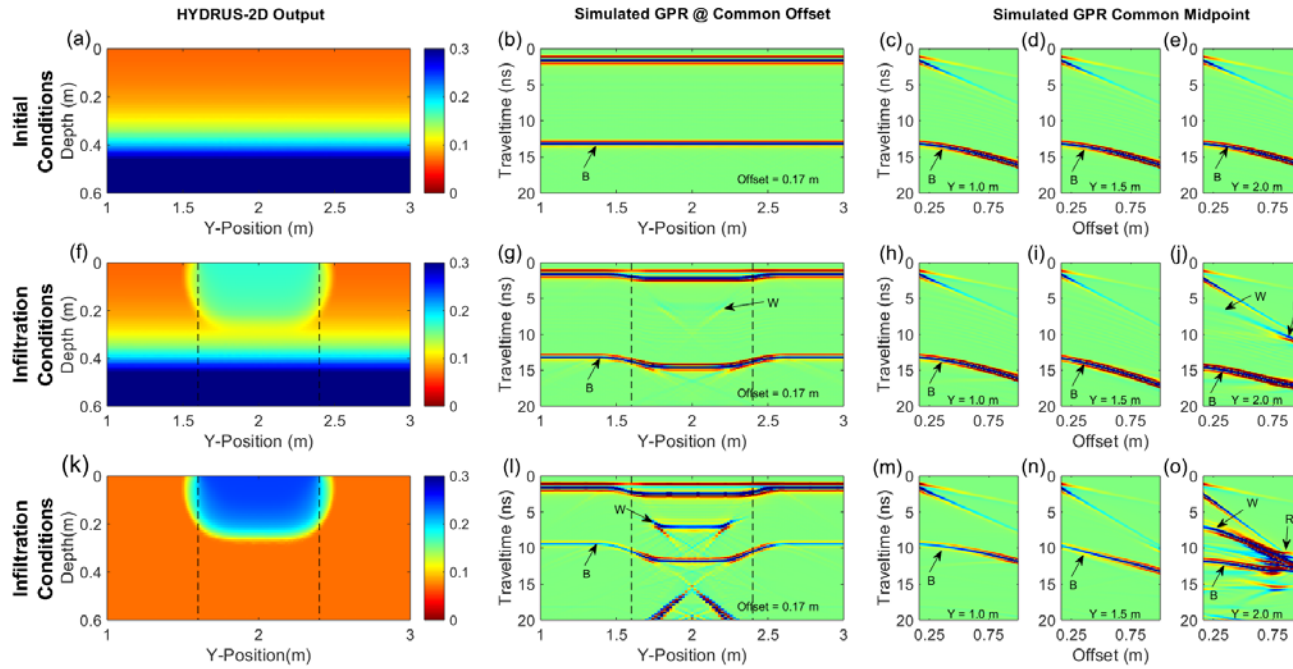
296 12(3), 1976.  
297 Neidell, N. S. and Taner, M. T.: Semblance and other coherency measures for multichannel data, *Geophysics*, 36(3),  
298 482–497, 1971.  
299 Nimmo, J. R.: Preferential flow occurs in unsaturated conditions, *Hydrol. Process.*, 26(5), 786–789,  
300 doi:10.1002/hyp.8380, 2012.  
301 Saintenoy, A., Schneider, S. and Tucholka, P.: Evaluating GroundPenetrating Radar use for water infiltration  
302 monitoring, 2007 4th Int. Work. on, Adv. Gr. Penetrating Radar, 91–95, doi:10.1109/AGPR.2007.386531, 2007.  
303 Sava, P. and Biondi, B.: Wave-equation migration velocity analysis. I. Theory, *Geophys. Prospect.*, 52(6), 593–606,  
304 doi:10.1111/j.1365-2478.2004.00447.x, 2004a.  
305 Sava, P. and Biondi, B.: Wave-equation migration velocity analysis — II : Subsalt imaging examples *Geophysical*  
306 *Prospecting*, , 1–36, 2004b.  
307 Simunek, J. and van Genuchten, M. T.: HYDRUS code for simulating the movement of water, heat, and multiple  
308 solutes in variably saturated porous media, 2005.  
309 Steelman, C. M. and Endres, A. L.: An examination of direct ground wave soil moisture monitoring over an annual  
310 cycle of soil conditions, *Water Resour. Res.*, 46(11), n/a-n/a, doi:10.1029/2009WR008815, 2010.  
311 Stork, C.: Reflection tomography in the postmigrated domain, *Geophysics*, 57(5), 680–692, doi:10.1190/1.1443282,  
312 1992.  
313 Topp, G. C., Davis, J. L. and Annan, A. P.: Electromagnetic Determination of Soil Water Content:, *Water Resour.*  
314 *Res.*, 16(3), 574–582, 1980.  
315 Vellidis, G., Smith, M. C., Thomas, D. L. and Asmussen, L. E.: Detecting wetting front movement in a sandy soil  
316 with ground-penetrating radar, *Am. Soc. Agric. Eng.*, 33(6), 1867–1874, 1990.  
317 Yilmaz, O. and Chambers, R.: Migration velocity analysis by wave-field extrapolation, *Geophysics*, 49(10), 1664–  
318 1674, 1984.  
319 Yilmaz, O. and Doherty, S.: *Seismic Data Analysis: Processing, Inversion, and Interpretation of Seismic Data*, 2nd  
320 ed., Society of Exploration Geophysicists, Tulsa, OK., 2001.  
321

322 8. Figures  
 323 Figure 1



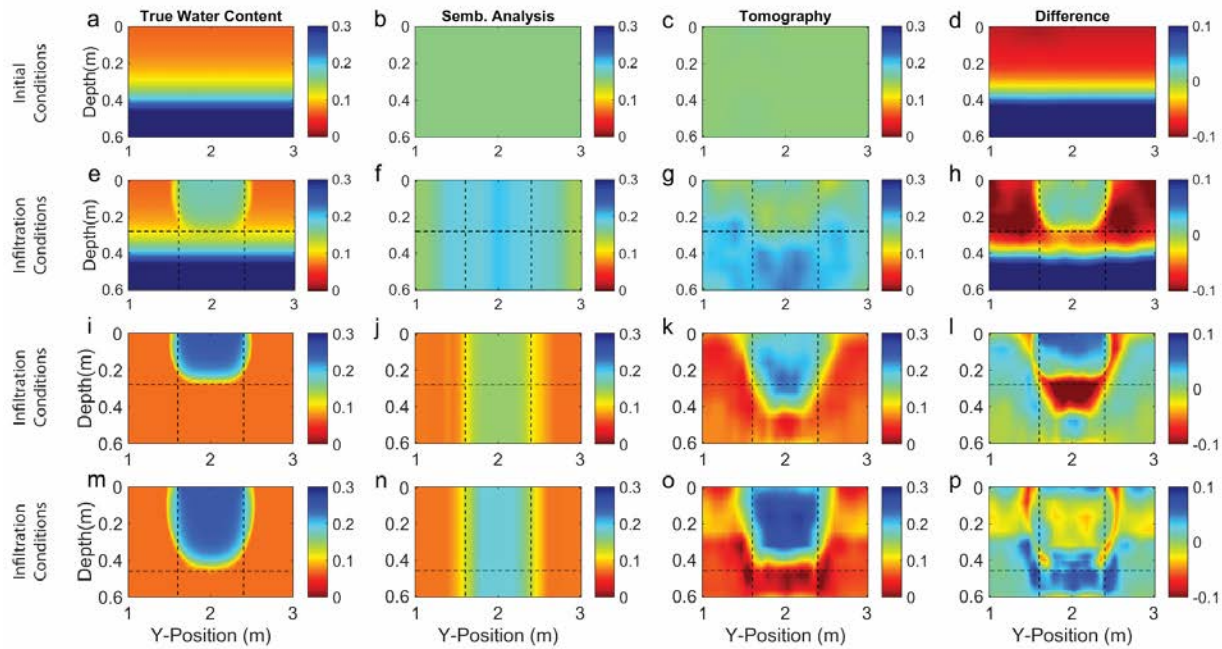
324  
 325 Figure 1: a) Example CMP data showing the airwave (A), groundwave (G) and reflection from a layer (B). Data in (a) is migrated to form (b) a migrated gather  
 326 with velocity 10% too slow; c) a migrated gather with correct velocity; and d) a migrated gather with velocity 10% too fast. Panel (e) shows a cross-section of the  
 327 experiment at  $y = 2.0$  m where  $t_1$ ,  $t_2$ , and  $t_3$  are arbitrary times during the infiltration. Panel (f) shows the plan-view of the experiment. Note that the bottom of the  
 328 sand layer is flat where GPR data collection occurs, i.e. on a boundary between drain cells, and pitched elsewhere toward cell drains.

329 **Figure 2**



330  
331 Figure 2: Panels (a), (f), and (k) show volumetric moisture distribution from HYDRUS-2D simulations used to generate simulated common-offset GPR data (b, g,  
332 l) and multi-offset GPR data (c-e, h-j, and m-o). Vertical dashed lines indicate the extent of the wetted surface. Annotated arrivals are the bottom of sand layer  
333 reflection (B), wetting front reflection (W), and refraction (R). Note that the base of sand reflection (B) is caused by the boundary at 0.60 m depth between the sand  
334 and gravel, not the capillary rise shown in panels (a) and (f).

335 **Figure 3**

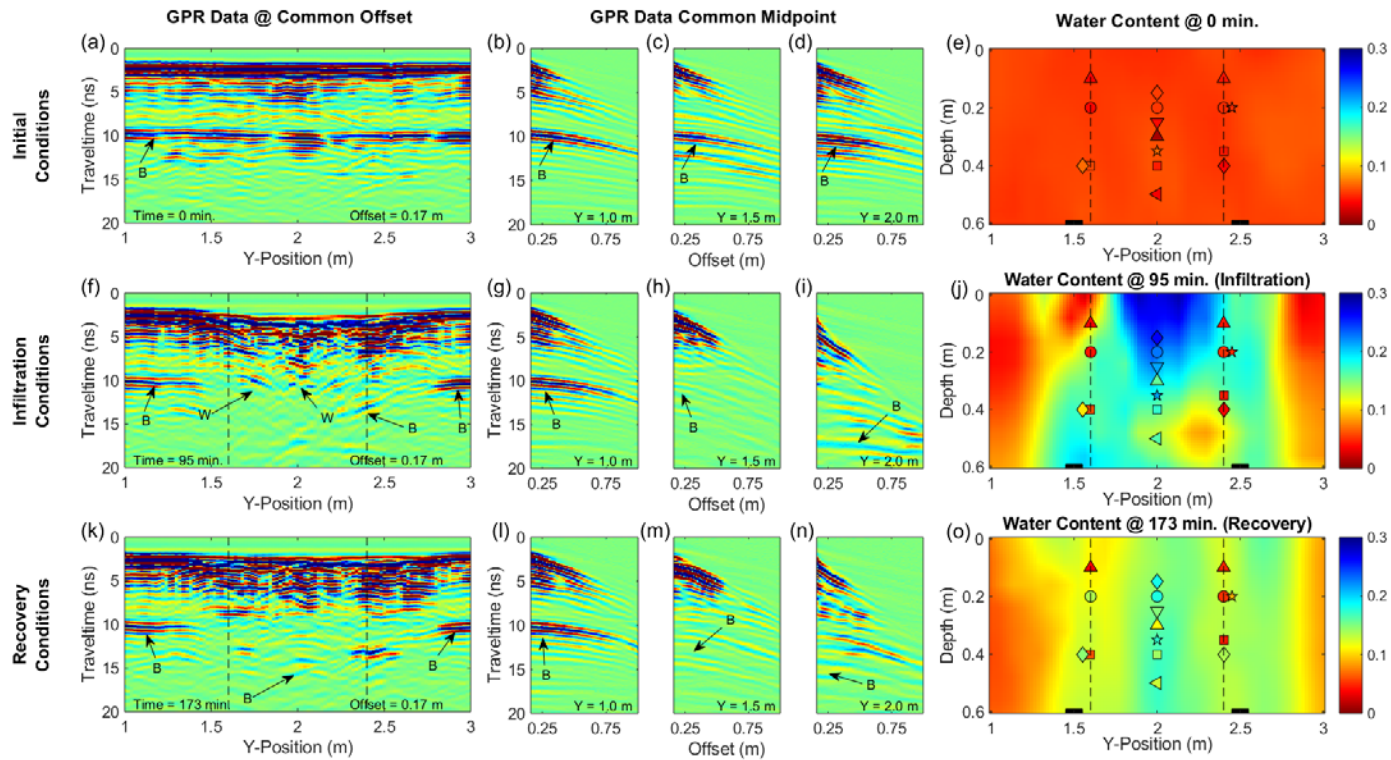


336

337 Figure 3: Panels (a), (e), (i), and (m) show true volumetric water content distributions from HYDRUS-2D. Panels (b), (f), (j), and (n) show starting models for the  
338 tomography derived from semblance analysis. Panels (c), (g), (k), and (o) show results of tomography of the simulated GPR data as volumetric water content.  
339 Difference plots (d), (h), (l), and (p) were calculated by subtracting the tomography results from the true water content distributions; red areas indicate volumetric  
340 moisture overestimation while blue areas indicate volumetric moisture underestimation.

341

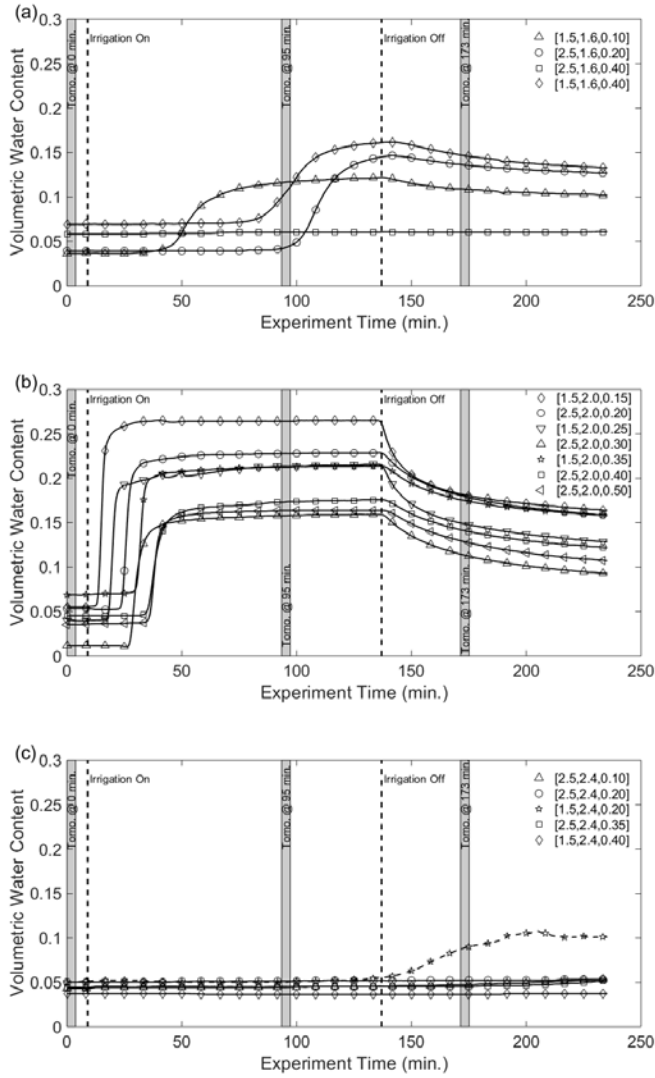




343

344 Figure 4: Panels (a, f, and k) are common-offset GPR data collected during the experiment. Panels (b-d, g-i, and l-n) are CMP data collected during the experiment.  
 345 Arrivals annotated are the sand layer reflection (B) and wetting front reflection (W). Panels (e, j, and o) show tomography results for the corresponding GPR data.  
 346 Vertical lines indicate the lateral extent of the wetted surface. Shapes correspond to the soil moisture data for the given y-location in Figure 5, colors correspond to  
 347 the measured soil moisture. Adjacent symbols are from probes that are located at different x-locations, but identical depths.

348 **Figure 5**



349  
 350 Figure 5: Soil moisture probe data from the in-situ moisture probes along the GPR line at a)  $y = 1.6$  m; b)  $y = 2.0$  m;  
 351 and c)  $y = 2.4$  m. Vertical dashed lines indicate the start and stop of irrigation. Gray bars indicate the times when data  
 352 in Figure 4 were collected. Symbols for a given data set match those on Figures 4e, j, and o. Soil moisture data were  
 353 collected 60 minutes beyond the end of GPR data collection.